Journal of Soils and Sediments (2019) 19:2089–2102
https://doi.org/10.1007/s11368-018-2193-y

SEDIMENTS, SEC 3 • HILLSLOPE AND RIVER BASIN SEDIMENT DYNAMICS • RESEARCH ARTICLE

The effects of rock fragment content on the erosion processes of spoil heaps: a laboratory scouring experiment with two soils

Jiaorong Lv[1,2] · Han Luo[1,3] · Jinsheng Hu[1,2] · Yongsheng Xie[3]

Received: 25 April 2018 / Accepted: 9 November 2018 / Published online: 23 November 2018

Abstract

Purpose Spoil heaps on newly engineered landforms create extensive artificially accelerated erosion, especially when there are catchment areas above spoil heaps, erosion caused by runoff will be much greater than that induced by rainfall. This study investigated the erosional characteristics of clay loam and sandy loam spoil heaps and proposed an appropriate hydraulic parameter to simulate the variation in erosion rate.

Materials and methods A laboratory scouring experiment was conducted using a soil pan (dimensions 5 m × 1 m × 0.5 m deep) with a discharging arrangement to test four samples of clay loam and sandy loam containing rock fragments (0%, 10%, 20%, and 30%) by mass. The slope of simulated spoil heaps was 53.2% with a discharging inflow rate of 15 L min^{-1}. The rock fragments used were those commonly used in construction works, having a diameter of 2–3 cm and irregular shape. Twenty-four scouring tests for eight treatments with duplication were accomplished in total.

Results and discussion Average erosion rates showed a negative linear correlation with rock fragment content in clay spoil heaps ($R^2 = 0.94$) and a positive linear correlation in sandy loam spoil heaps ($R^2 = 0.92$). Rill width evolution of clay loam spoil heaps mainly developed at the early scouring stage (0–15 min), and rills developed even more rapidly during later scouring times (30–60 min) in sandy loam spoil heaps. Grey relational analysis showed that sheer stress and stream power both had higher Grey relational degrees with erosion rate for both soils, regression analysis showed that stream power can efficiently describe the erosional process of clay loam and sandy loam for each rock fragment content, but sheer stress only did well in sandy loam heaps.

Conclusions Adding rock fragments to spoil heaps resulted in significantly opposite effects in the different soils; great attention should be paid to sandy loam spoil heaps due to their more severe erosion with increasing rock fragment content; stream power is an appropriate hydraulic parameter to simulate the soil erosion process of spoil heaps for both soil types.

Keywords Hydraulic parameter · Laboratory scouring experiment · Rill erosion · Rock fragment content · Spoil heaps

1 Introduction

Intense erosion acceleration of engineering-disturbed land surfaces has received increasing attention in recent years. Such erosion causes serious environmental problems, deteriorates the ecological environment, and reduces land productivity (Tommervik et al. 2012; Trenouth and Gharabaghi 2015; Nearing et al. 2017). Spoil heaps (e.g., spoil banks formed in the preparation, construction, and operation periods of construction activities, which contain excavated soil, rock fragments, construction waste materials, and slags) are the source of severe soil loss on engineered land surfaces (Gilley et al. 1977; Hancock et al. 2008; Peng et al. 2014). In many cases, they are formed when spoil is dumped onto steep slopes, especially during linear construction programs such as

Responsible editor: Rajith Mukundan

Han Luo contributed equally to this work and should be considered as co-first author.

✉ Yongsheng Xie
ysxie@ms.iswc.ac.cn

[1] Institute of Soil and Water Conservation, Chinese Academy of Sciences and Ministry of Water Resources, Yangling 712100, Shaanxi, China

[2] University of the Chinese Academy of Sciences, Beijing 100049, China

[3] Institute of Soil and Water Conservation, Northwest A&F University, Yangling 712100, Shaanxi, China

expressway or railway construction and road building (Harbor 1999; Nyssen et al. 2002; Zhang et al. 2015), increasing the catchment size and causing gullying at most of the culverts and other road drains (Nyssen et al. 2002). The steep slope, loose structure, and low vegetation cover lead to the soil of spoil heaps being easily eroded (Gilley et al. 1977). Areas disturbed by construction activity have a soil erosion rate from two to 40,000 times greater than pre-construction conditions and are important components of non-point source pollution that degrades surface water quality (Harbor 1999). According to the China's Ministry of Water Resources survey released, the amount of soil loss on engineering-disturbed land surfaces reached 946 million tons over areas totaling 5.528×10^6 hm^2 in China during 2001–2005; worse still, in 2006–2010, these figures increased by 11.5% over the previous 5 years, leading to serious soil and ecological degradation.

Rock fragments are a significant component of spoil heaps. Peng et al. (2014) roughly classified spoil heaps into *partial soil* (soil/rock ratio 4:1) and *rocky* (soil/rock ratio 3:2) spoil heaps. Field and laboratory studies have shown that the rock fragment content has a great impact on soil properties and on the hydrological and erosional processes of the original surfaces (Rieke-Zapp et al. 2007; Zhou et al. 2011; Nasri et al. 2015). Jomaa et al. (2012) shows that rock fraction affects runoff generation and erosion patterns. Nasri et al. (2015) indicated that the presence of rock fragments produces preferential flow channels in clay loam soil by increasing macropores, meanwhile impermeable rock fragments increase pore tortuosity, which extends the path of soil water movement (Zhou et al. 2011) to decrease water infiltration. The content of rock fragments can influence soil hydrological processes by affecting how the quantity of macropores and the tortuosity change (Ma and Shao 2008) and further influence soil erosion. Some studies (Chow and Rees 1995; Urbanek and Shakesby 2009) indicated that infiltration increased and runoff generation and soil loss decreased when rock fragment content increased. But, some studies showed content thresholds of rock fragment on the changes of corresponding hydrological, such as the critical content to be 40% where the saturated hydraulic conductivity is smallest in Zhou et al. (2009) and the 15% volumetric content where the steady effluent reached its maximum in Shi et al. (2012). So, the impact of rock fragments on soil hydrological varied between different experimental conditions and needs to be addressed for a given situation.

Moreover, the conclusion of Rieke-Zapp et al. (2007) suggested that rock fragments dissipate the energy in the flow path on a 5-mm-deep V-shaped flume surface; thus, soil loss exhibits a linear reduction with increasing rock fragment content (0–40%). Some studies (Nyssen et al. 2001; Rieke-Zapp et al. 2007; Guo et al. 2010) also showed that rock fragments resting on the soil surface protect topsoil from detachment and the impact of raindrops and reduce physical degradation of the soil surface based on the increase in water flow resistance and friction factor. Therefore, the rock fragments play complex roles in affecting soil hydrological and erosion processes. However, few studies have focused on the extent to which rock fragment content affects the erosional mechanisms and hydraulic properties of spoil heaps for different soil types. Runoff generation and sediment yield have been shown to be affected by rock fragment content in disturbed soil (Peng et al. 2014), but the erosional mechanism of spoil heaps with different rock fragment contents still requires clarification.

Prediction of the amount of soil lost from the engineering-disturbed land surface is essential to allocate reasonable soil and water conservation measures to reduce such loss. Kayet et al. (2018) evaluated the soil loss in hillslope mining areas using the revised universal soil loss equation (RUSLE) model, which is an empirical model and suitable for watershed scale. But, Zhang et al. (2015) indicated that the empirical–statistical models based on the USLE framework (Wischmeier and Smith 1978) were found to be of large uncertainty because of model conceptualization as well as arbitrary choice of model parameter. Moreover, due to the lack of dynamical located observations of spoil heaps in details over a long term, the model factor localization dedicated to spoil heaps is difficult to achieve, especially for the soil containing rock fragments, RUSLE have limited usage. Constructing process-based prediction models is an important way to estimate soil loss efficiently, for which using simple hydraulic indicators is an effective and general approach for practical application (Knapen et al. 2007; Basile et al. 2010). Therefore, laboratory experiments are needed to understand the dynamic erosion process in order to clarify the suitable parameter for simulating spoil heap erosion.

Several hydraulic parameters (shear stress, stream power, unit stream power) are commonly used to estimate soil detachment and the critical conditions for soil erosion, e.g., the Water Erosion Prediction Project (Nearing et al. 1989), the Griffith University Erosion System Template (Misra and Rose 1996), and the European Soil Erosion Model (Morgan et al. 1998). Although some ecologists have noted that stream power (ω) is the more significant (Zhang et al. 2015; Wang et al. 2016) for characterizing hydrodynamic mechanisms of spoil heap erosion, they did not take the effect of rock fragment content into account; besides, the great differences in the test conditions of these studies give poor comparability and utility of their results. The conclusions of in situ scouring tests (Zhang et al. 2015) cannot be generally applied for its greater dependence on the in situ soil conditions and scale of the tests; the reduced-scale representation of actual cone-shaped spoil heaps that Wang et al. (2016) used in simulated rainfall experiments is judged to be too small (slope length is 1.1 m) to simulate forms of erosion other than splash and sheet, such as rill erosion.

Weak structural stability and the complicated effects of rock fragments lead to a great difference in hydrological and erosional characteristics between undisturbed slopes and spoil heaps. The optimal parameter that best reflects the runoff and erosional characteristics of the spoil heaps containing rock fragments still remains to be discussed. Consequently, what required to be investigated presently are the determination of runoff and erosional characteristics of spoil heaps with different rock fragment concentrations for different soil types and the identification of the best parameter that best reflects this through reproducible tests having better control and simulation accuracy. Thus, a laboratory experiment was conducted in this study under controlled conditions with the specific objectives of

(1) Investigating the sediment yielding process in two kinds of engineering spoil heap, each consisting of one particular soil type containing different rock fragment contents, using upper overflow scouring;
(2) Evaluating the relationships between five hydraulic parameters and soil erosion rate, then proposing the best parameter for use in modeling to simulate the soil erosion processes in spoil heaps.

2 Materials and methods

2.1 Materials and equipment

A survey of 368 spoil heaps on disturbed land surfaces by Zhao et al. (2012) showed that most of the slope gradients of spoil heaps were between 48.8 and 70.0% and slope lengths were mostly in the range from 2 to 8 m. In the present study, a 53.2% slope and 5 m length were chosen as the design shapes of the spoil heaps to be tested. The tests of spoil heaps formed in clay loam (Fig. 1) and sandy loam (Fig. 2) areas of the water erosion region in China were conducted in the study. Field surveys also showed that more than 90% of actual spoil heaps

Fig. 1 Photograph of a typical engineering spoil heap in a clay loam area

Fig. 2 Photograph of a typical engineering spoil heap in a sandy loam area

contain less than 40% by mass of rock fragments (Kang et al. 2016); therefore, four rock-fragment content mass percentages (0%, 10%, 20%, 30%) were investigated in the experiment. Consideration of the discharge per unit width produced in an experimental plot for typical erosive rainstorm in the study area (rainfall intensity is 120 mm h^{-1} (Fang et al. 2015), and recurrence interval is 100–150 a) led to a design inflow rate of 15 L min^{-1} (Peng et al. 2014).

The indoor runoff scouring experiment was conducted in the rainfall simulation laboratory at the State Key Laboratory of Soil Erosion and Dryland Farming on the Loess Plateau, Yangling City, China, using clay loam from Nanchang, Jiangxi Province, and sandy loam from Jingbian, Yulin, Shanxi Province, China. The bulk soil was gently crushed and passed through a 6-mm sieve before soil pan preparation. The mechanical compositions of the two soils were determined using a Mastersizer 2000 laser particle size analyzer (Malvern Panalytical, Malvern, UK). The results are listed in Table 1. The rock fragments used were those commonly used in construction works, having a diameter of 2–3 cm and irregular shape.

As shown in Fig. 3, the water scouring supply consisted of an adjustable stabilizing water pump, a pipe, an overflow tank, and an experimental soil pan with an adjustable slope gradient (dimensions 5 m × 1 m × 0.5 m deep) with a collecting groove at the end of the pan to collect sediment samples. Water was pumped into the overflow tank and then flowed from the discharge wall of the tank in a uniform thin layer. Numerous small holes in the bottom of the pan allowed the soil to drain naturally.

Table 1 Mechanical compositions of the two soils (%)

Size (mm)	< 0.002	0.002–0.02	0.02–0.05	0.05–0.10	0.1–2.0
Clay loam	19.66	37.96	18.68	23.63	0.17
Sandy loam	5.895	10.196	26.266	35.800	21.844

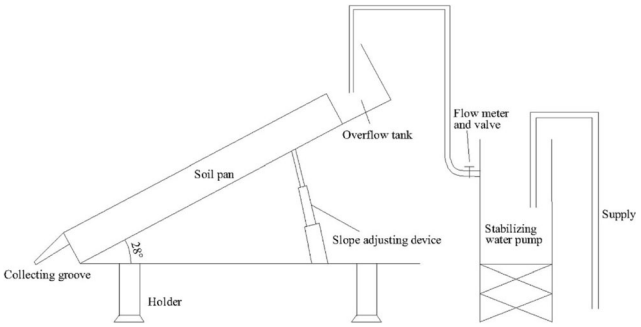

Fig. 3 Scouring experimental system

Prior to packing the soil pan, the bulk densities of the rock fragments and soil were determined to be used to calculate the quantities needed to obtain the target rock fragment content and bulk density of each soil layer. Then, these amounts of gravel and soil were mixed evenly and packed layer by layer. The bottom layer of 5-cm-thick sand with a gauze covering (to allow water to drain from the soil) was overlain by a 15-cm-thick soil layer, artificially compacted to simulate the original slope before the spoil had been dumped. The bulk density of this layer was approximately 1.9 g cm^{-3} (error < 10%). The uppermost layer comprised an uncompacted 30 cm thickness of uniformly mixed soil-rock fragment aggregate similar to the designed rock fragment content to simulate the dumped spoil. The surface was then smoothed, and the soil was soaked using a handheld spray until surface flow occurred to saturate the soil (slightly less than 25% moisture content for the sandy loam; slightly more than 25% moisture content for the clay loam) to reduce any spatial variation between treatments in the simulated spoil heaps that may have been caused by packing. The soil pan was then covered with a plastic sheet to seal the surface and prevent evaporation and allowed to settle for 24 h.

2.2 Experimental procedures

Two soils (clay loam and sandy loam) and four rock fragment contents (0%, 10%, 20%, and 30% by mass) were investigated. All the treatments were repeated three times, with 24 scouring tests conducted in total. The water inflow rate was calibrated before each test to 15 L min^{-1} (error < 5%). The plastic sheet was then removed to let the slope surface be subjected to the sheet flow of water. When more than 80% of the slope area began to generate runoff, the test was initiated and the timer was started. During the test, four 1-m-long observation sections were set from upslope (0.5 m) to downslope (4.5 m). A dye method (coloration by $KMnO_4$ solution) was used to measure flow velocity (the average of the measured values on the four sections multiplied by the error correction factor of 0.75) (Li et al. 1996). The width of each flow path and the rill shapes (width, depth, length) were measured in the four sections using a ruler. The average was taken as the value for the whole surface. All measurements were performed at the same intervals of sediment sampling. Sediment samples were collected in 5-L buckets every 1 min for the initial 3 min, then every 3 min until the test was complete. Each sampling time was between 5 and 15 s. Every scouring test lasted 60 min, producing 22 samples. After each test, the sample volumes were measured and the sediments were oven-dried at 105 °C for at least 24 h. Sediment yields were then calculated.

2.3 Equations and data analysis

2.3.1 Hydraulic parameters

Flow depth is an essential parameter for calculating the other hydraulic parameters, but unfortunately, it is very difficult to measure because of its dynamic condition and submillimeter scale along the slope. Assuming the slope flow is uniform, the average flow depth can be calculated from

$$h = \frac{q}{bv} \tag{1}$$

where h is the flow depth (m), q is the instantaneous runoff yield ($m^3\ s^{-1}$), b is the average width of flow path (m), and v is the flow velocity (m s^{-1}).

Erosion rate is given by

$$E_r = \frac{M}{BLt} \tag{2}$$

where E_r is the erosion rate (g $m^{-2}\ s^{-1}$), M is the sediment sample weight (g), B is the slope width (m), L is the slope length (m), and t is the sampling time (s).

The hydraulic parameters used in the study were the shear stress (τ, Pa), stream power (ω, N $m^{-1}\ s^{-1}$), unit stream power (P, m s^{-1}), unit energy of water-carrying section (E, m), and Darcy-Weisbach roughness coefficient (f). The shear stress is given by

$$\tau = \rho_m g R J \tag{3}$$

where ρ_m is the water-sediment mixture density (kg m^{-3}); g is the acceleration due to gravity (m s^{-2}); J is the hydraulic gradient, which is approximately equal to the sine of the slope gradient; and R is the hydraulic radius (m), given by

$$R = \frac{bh}{2h + b} \tag{4}$$

Stream power is calculated by

$$\omega = \tau v \tag{5}$$

Unit stream power is given by

$$P = vJ \tag{6}$$

The unit energy of the water-carrying section is given by

$$E = \frac{av^2}{2g} + h(a = 1) \tag{7}$$

The Darcy-Weisbach roughness coefficient is calculated from

$$f = \frac{8gRJ}{v^2} \tag{8}$$

2.3.2 Grey relational analysis

In this study, the degrees of correlation between the hydraulic parameters and erosion rate were evaluated using the Grey relational analysis (GRA) (Deng 1989), which is the most widely used component of Grey system theory in information theory for its less strict requirement of sample size or typical statistic distribution and the light labor of calculation. It provides a straightforward approach for analyzing the influence of different factors on the target factor based on time series, even where little information is available. The essence of GRA is quantitative comparison of dynamic development trends of factors in the system. The procedure in the present study was as follows:

(1) The factor series were collected, taking the erosion rate series as the reference sequence (X_0). The comparison sequences (X_i) were the five hydraulic parameter series. Specially, the reciprocal of f (the Darcy-Weisbach function) was used here considering that greater values of f generally indicated that more runoff energy is needed to overcome the resistance of surface roughness, with a consequently smaller sediment yield (Peng et al. 2014). These are expressed as

$$X_0 = \{x_0(k)\}, k = 1, 2, \ldots, n \tag{9}$$

$$X_i = \{x_i(k)\}, k = 1, 2, \ldots, n; i = 1, 2, \ldots, m \tag{10}$$

(2) Data standardization: before calculating the Grey relational coefficient, series data must be standardized because of the different units. Here, the original series are standardized as

$$x_0'(k) = \frac{x_0(k)}{\frac{1}{n}\sum_{k=1}^{n} x_0(k)}, x_i'(k) = \frac{x_i(k)}{\frac{1}{n}\sum_{k=1}^{n} x_i(k)} \tag{11}$$

(3) Calculation of absolute values ($\Delta_{0i}(k)$): $\Delta_{0i}(k)$ is the absolute value of the difference between X'_0 and X'_i in k units expressed as

$$\Delta_{0i}(k) = |X_0'(k) - X_i'(k)| \tag{12}$$

$$\Delta_{\min} = \min_0 \min_i \Delta_{0i}(k) \tag{13}$$

$$\Delta_{\max} = \max_0 \max_i \Delta_{0i}(k) \tag{14}$$

(4) The Grey relational coefficient of X'_i and X'_0 is defined in k units as follows:

$$\xi_{0i}(k) = \frac{\Delta_{\min} + \beta\Delta_{\max}}{\Delta_{0i}(k) + \beta\Delta_{\max}} \tag{15}$$

where β is a distinguishing coefficient ($\beta \in [0, 1]$) that is used to weaken the effect of extreme values of $\Delta_{\max}$ which would distort the correlation coefficient; a value of 0.5 is generally adopted.

(5) The Grey relational degree is the average of the series of Grey relational coefficients. The Grey relational degree for the X_i series is given by

$$\gamma_{0i} = \frac{1}{n}\sum_{t=1}^{N} \xi_{0i}(k) \tag{16}$$

2.3.3 Model evaluation

The performances of each of the regression equations obtained in this study were evaluated by the coefficient of determination (R^2), the normalized root mean square error (NRMSE), and the Nash-Sutcliffe model efficiency coefficient (NSE).

The R^2 value indicates the percentage of the variation of the dependent variables that can be explained by the relationship and is given by

$$R^2 = \frac{\left[\sum_{i=1}^{n}\left(X_{o,i} - X_{o,avg}\right) \times \left(X_{p,i} - X_{p,avg}\right)\right]^2}{\sum_{i=1}^{n}\left(X_{o,i} - X_{o,avg}\right)^2 \times \sum_{i=1}^{n}\left(X_{p,i} - X_{p,avg}\right)^2} \tag{17}$$

The NRMSE represents the deviation of the measured value from the predicted value and is given by

$$\text{NRMSE} = \frac{\sqrt{\frac{\sum_{i=1}^{n}\left(X_{o,i} - X_{p,i}\right)^2}{n}}}{X_{o,avg}} \tag{18}$$

The NSE indicates how well the observed versus simulated values fit the 1:1 line

$$\mathrm{NSE} = 1 - \frac{\sum_{i=1}^{n}\left(X_{\mathrm{o},i} - X_{\mathrm{p},i}\right)^2}{\sum_{i=1}^{n}\left(X_{\mathrm{o},i} - X_{\mathrm{o,avg}}\right)^2} \quad (19)$$

In Eqs. (17) to (19), $X_{\mathrm{o},i}$ is the observed values, $X_{\mathrm{p},i}$ is the predicted values, $X_{\mathrm{o,avg}}$ is the mean observed value, and $X_{\mathrm{p,avg}}$ is the mean predicted value. The closer R^2 and the NES are to 1 and the closer the NRMSE is to 0, the better the performance of the equation in establishing the relationship.

2.4 Data analysis

The statistical analysis was performed using IBM SPSS (version 23.0) software (IBM Corp., Armonk, NY, USA) using a significance level of 0.05, and graphs were plotted by OriginPro® (version 9) software (OriginLab®, Northampton, MA, USA). For the hydraulic parameters, 90% of the data was randomly selected to establish the equations, and the remaining 10% was used to validate them.

3 Results

3.1 Runoff rate and erosion rate change

3.1.1 Runoff rate

Runoff is the driving force of soil erosion and the carrier of sediment transporting. The changes in runoff for different treatments are plotted in Fig. 4. Runoff rate gradually increases at the beginning because of the lower water content and larger infiltration capacity of soil. With the soil becoming saturated, runoff rate tended to be constant. The time when runoff rate turned to be stable was around 10 min for clay loam and 30 min for sandy loam which indicated a stronger infiltration capacity of sandy loam. Moreover, the runoff rates for both soil types showed fluctuations which could be mainly attributed to the rill formation processes. The undercutting of rills and random collapse of rill side wall could block the flow path which caused the fluctuation of runoff rate.

The relationship of total runoff volume and total sediment yield with rock fragment content varied for the two soils as displayed in Fig. 5. Overall, the average total runoff volume of clay loam was 3.5% less than that of sandy loam heaps. Runoff was promoted by adding rock fragments in sandy loam but impeded in clay loam spoil heaps, and total runoff volume had a positive relationship with the total sediment yield for both soil types ($R^2 = 0.91$ and 0.75).

3.1.2 Erosion rate

Erosion rate is an important forecasting parameter in process-based models. In this experiment, the change trends of erosion rate with time were obtained by measuring and analyzing sediment samples of each treatment (Fig. 6).

The erosion rates in the ranges 0.94–39.47 g m^{-2} s^{-1} and 8.87–57.05 g m^{-2} s^{-1}, respectively, were found for clay loam and sandy loam spoil heaps, which both fluctuated greatly throughout the scouring time. For clay loam spoil heaps (Fig. 6), the erosion rates for each treatment fluctuated within a range without any apparent trend during the scouring process except that the erosion rate of heap containing 20% and 30% rock fragment changed stably at a lower level in the last 20 min. For sandy loam spoil heaps, erosion rates of rocky treatments changed smoothly before 18 min, after which they increased for about 20 min, then erosion rates fluctuated around relatively higher values; a similar trend of erosion rate evolution of bare soil heap was not as straightforward as rock spoil heaps, but the erosion rate after 30 min was still slightly higher than the previous 30 min. The obvious increase phase of sandy loam erosion rate implies an apparently intense development of rills centered in the mid-term of scouring, which

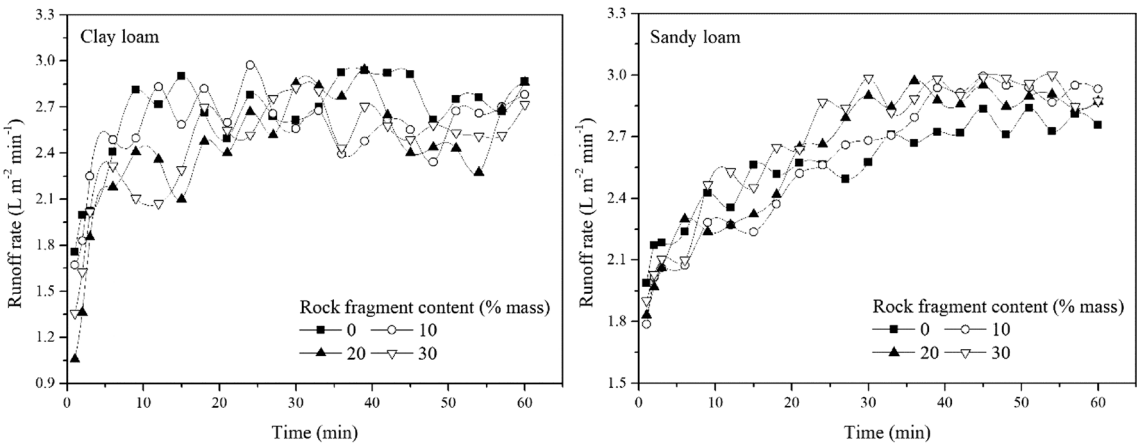

Fig. 4 Change in runoff rate with time for four values of rock fragment content

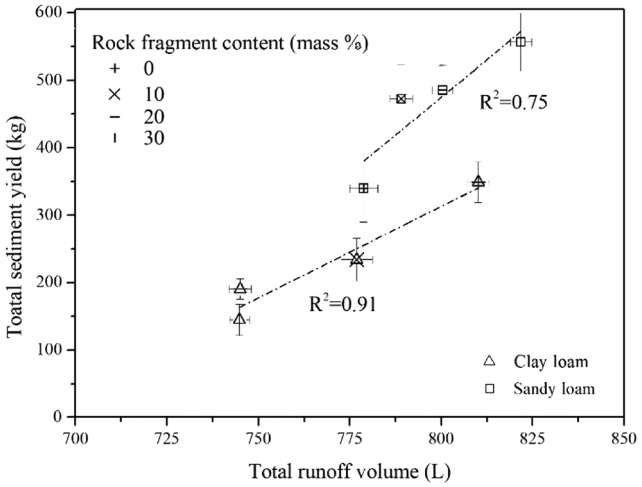

Fig. 5 Relationship between total runoff volume and total sediment yield for the four rock fragment content

Fig. 7 Overview of soil surface after scouring simulation. **a** Clay loam spoil heaps with 30% rock fragments. **b** Sandy loam spoil heaps with 30% rock fragments. **c**, **d** First observation sections of slopes in **a** and **b**, respectively. Clay loam spoil heaps had less broken surface and a more stable side wall than sandy loam spoil heaps

shows that the erosion rate increased at the greatest rate when rill erosion became the dominant pattern; for clay loam, there was no such dramatic development of rill erosion. Erosion rates for clay loam spoil heaps containing 20% and 30% rock fragments changed at relatively lower levels in the last 21 min, and those of sandy loam spoil heaps with 10–30% rock fragments decreased for 15–20 min finally. This indicates that the gradually increasing rock surface cover available as soil was detached helped to reduce soil erosion (Fig. 7) (Rieke-Zapp et al. 2007).

Although erosion rate evolution curves did not vary visibly for the different rock fragment contents, it had a significant effect on erosion rates ($*p < 0.05$). The average erosion rates of all treatments are plotted in Fig. 8. Average erosion rates for clay loam and sandy loam spoil heaps were 8.24–18.55 g m^{-2} s^{-1} and 19.33–29.55 g m^{-2} s^{-1}, respectively. It is apparent that the average erosion rate decreased with increasing rock fragment content in clay loam, and the opposite occurred in sandy loam (Fig. 8). When rock fragment content was increased from 0 to 30%, the average erosion rate decreased by 55.6% for clay loam and increased by 52.8% for sandy loam. The addition of rock fragments had exactly the opposite effect on the erosion rate of the two different soils in the spoil heaps. This supports the idea that, at least to some extent, increasing the rock fragment content protected clay loam spoil heaps from erosion but led to the deterioration of sandy loam spoil heaps.

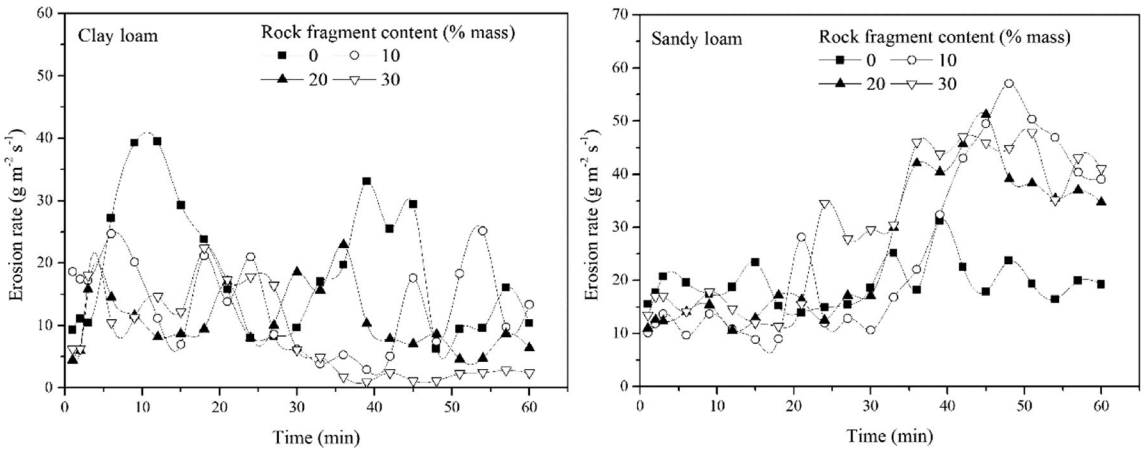

Fig. 6 Change in erosion rate with time for four values of rock fragment content

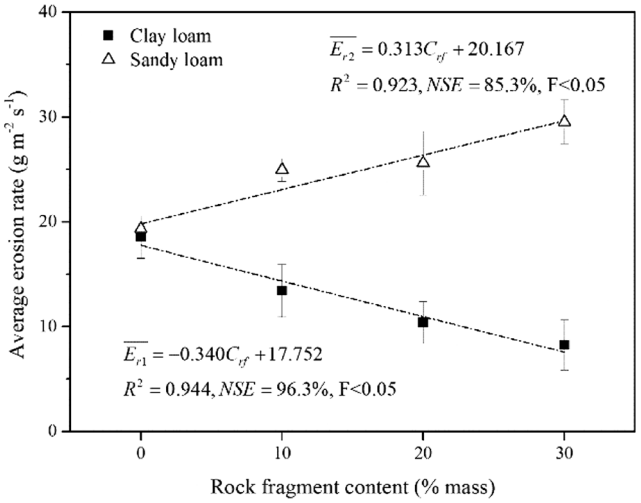

Fig. 8 Average erosion rate for four rock fragment contents in clay loam spoil heaps and sandy loam spoil heaps. C_{rf} is the rock fragment content (% mass), E_{r1} is the erosion rate of clay loam spoil heap (in g m^{-2} s^{-1}), and E_{r2} is the erosion rate of sandy loam spoil heap (in g m^{-2} s^{-1})

On the whole, the difference between the average erosion rates for clay loam and sandy loam spoil heaps was rising with the increasing rock fragment fraction. In spoil heaps consisting only of soil, the average erosion rate of clay loam was 4.1% lower than for sandy loam; once rock fragment contents were 40%, the difference was 72.1% lower. Linear relationships were found between the average erosion rates and rock fragment contents for both soil types (Fig. 8). The slopes (− 0.340 for clay loam and 0.313 for sandy loam) demonstrated the two distinct effects of rock fragment content on erosion of the two soils which was consistent with the runoff variations.

3.2 Rill development

Based on experimental observation, rill incision (gully formation) began after 3 min of scouring during the experiment. It is conceivable that rill erosion plays an important role in the erosion process of spoil heaps. At the end of each test, the slope surface tended to be highly broken (Fig. 7) rather than the rills being aligned parallel to the direction of flow as might be expected. Therefore, it was not easy to measure the exact rill lengths and depths. Because the rock fragments prevented undercut erosion, rill deepening was not obvious. Nevertheless, to some extent, the rill width mirrored the degree of incision of the slope surface, defined here as the average rill width of the four observed sections.

To provide an overall understanding of rill erosion development for different rock fragment contents, the cumulative effect of each treatment was analyzed at four time intervals: 0–15 min, 0–30 min, 0–45 min, and 0–60 min (cumulative flow discharge volume 225 L, 450 L, 675 L, and 900 L, respectively). Figure 9 shows that rill development was less severe in the clay loam spoil heaps than in the sandy loam spoil heaps. Increasing the rock fragment content hindered the widening of the rills in the clay loam spoil heaps but exacerbated it in sandy loam (Fig. 10), consistent with the observed changes in erosion rate.

Based on scouring times, the average widening rates were 4.0–5.9 mm min^{-1} for the clay loam and 6.3–9.5 mm min^{-1} for the sandy loam spoil heaps. In the latter periods of the tests (30–60 min, Fig. 9), the line slope of soil-rock mixture decreased by 38.0% for clay loam but increased by 27.4% for sandy loam, indicating that rills mainly developed in the clay loam spoil heaps in the early period, but for sandy loam spoil heaps, the rills developed more intensely in the later stages. This also confirms the rise of erosion rate evolution in the sandy loam evident in Fig. 6. Figure 9 also implies that large-scale rill expansion caused a notable rise in erosion rate for the sandy loam spoil heaps but was less common in the clay loam spoil heaps.

As rock fragment content increased, the total sediment yield changed in concordance with the final rill width (Fig. 10). The final rill width ranges of the four rock fragment

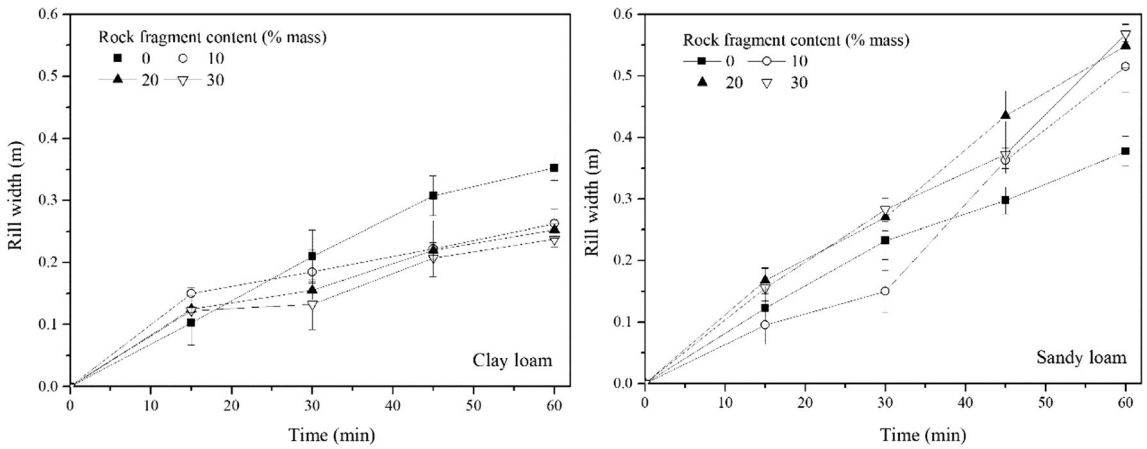

Fig. 9 Rill width evolution for different rock fragment contents

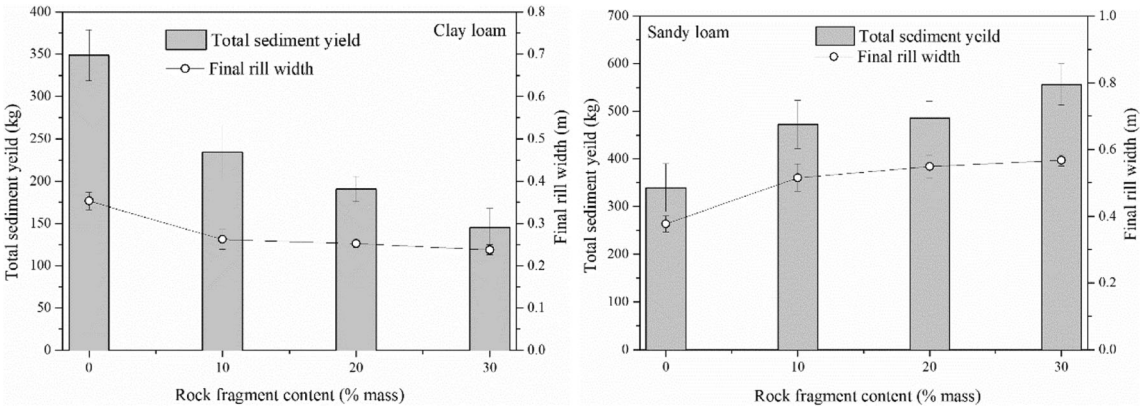

Fig. 10 Total sediment yield and final rill width change for different rock fragment contents

contents were 0.24–0.35 m for clay loam spoil heaps and 0.38–0.56 m for sandy loam spoil heaps. For the sandy loam spoil heaps with 30% of rock fragments, the channels (0.56 m wide) occupied more than half of the slope width, reflecting the severity of the destruction of the spoil heap slope, with an average final rill width 2.4 times that of the clay loam rills and a total sediment yield 1.9 times larger.

For each soil type, the final rill width differences became less obvious as the proportion of rock fragment content was increased: an increase from 10 to 30% resulted in a rill width decrease of 0.03 m for clay loam and an increase of 0.04 m for sandy loam. However, for no-rock-content spoil heaps to soil-rock fragment mixtures, the rill width gaps rose to 0.09 m for clay loam and 0.14 m for sandy loam, suggesting that the presence of rock fragments in the different soils did indeed have a significant effect on rill erosion development, but the differences were less noticeable with increasing rock fragment content.

3.3 Relationships between erosion rate and hydraulic parameters

The GRA is used to analyze the degrees of effects of effective factors on a selected target factor based on a geometrical approach. The GRA was used in this study to assess the influence of hydrodynamic parameters on erosion rate throughout the erosion process on the surface of spoil heaps.

Under each treatment, the erosion rate (X_0) was sequenced chronologically as the corresponding flow shear stress (X_1), stream power (X_2), and unit stream power (X_3); the reciprocal of f (the Darcy-Weisbach function) (X_4); and the unit energy of water-carrying section series (X_5). The matrix of correlation coefficients for the two soil types is shown in Table 2. As can be seen, sheer stress (X_1) and stream power (X_2) both had greater Grey relational degrees with erosion rate (X_0) of the five parameters for both soil types ($\bar{\gamma}_{01}$ = 0.665 and 0.680; $\bar{\gamma}_{02}$ = 0.677 and 0.690, respectively), indicating that they both may potentially be the preferred descriptors of the erosional process. The paired t test was made to sheer stress and stream power parameters for each soil type, and the results showed that the difference between the two parameters for clay loam is not significant ($^*p = 0.070$) but significant for sandy loam ($^*p = 0.015$).

The sheer stress/erosion rate and stream power/erosion rate pairs are plotted in Fig. 11, and regression analysis was conducted between each parameter and erosion rate; the best fit equations are shown in Table 3. Linear equation was the best form to describe the relationships between the two parameters and erosion rate for both soils. The statistical evaluation implied that for clay loam, only stream power could model the erosion rate change effectively, but for sandy loam, both parameters were good predictors with satisfactory R^2, NSE, and NRMSE values. Figure 10 also shows the fitting results visually.

Stream power decreased for clay loam and increased for sandy loam with larger proportions of rock fragments (Fig. 11), consistent with the changes of detachment rates. The coefficient of stream power in the equations was

Table 2 Grey correlation coefficients of soil erosion rate and hydraulic parameters for spoil heaps for the four values of rock fragment content

Soil	Rock fragment content (% mass)	γ_{01}	γ_{02}	γ_{03}	γ_{04}	γ_{05}
Clay loam	0	0.645	0.688	0.611	0.593	0.670
	10	0.666	0.642	0.600	0.615	0.547
	20	0.705	0.699	0.681	0.641	0.651
	30	0.642	0.679	0.704	0.635	0.635
	$\bar{\gamma}_{0i}$	0.665	0.677	0.649	0.621	0.626
Sandy loam	0	0.670	0.692	0.725	0.656	0.703
	10	0.697	0.710	0.621	0.579	0.608
	20	0.677	0.695	0.649	0.691	0.606
	30	0.678	0.661	0.515	0.503	0.501
	$\bar{\gamma}_{0i}$	0.680	0.690	0.628	0.607	0.605

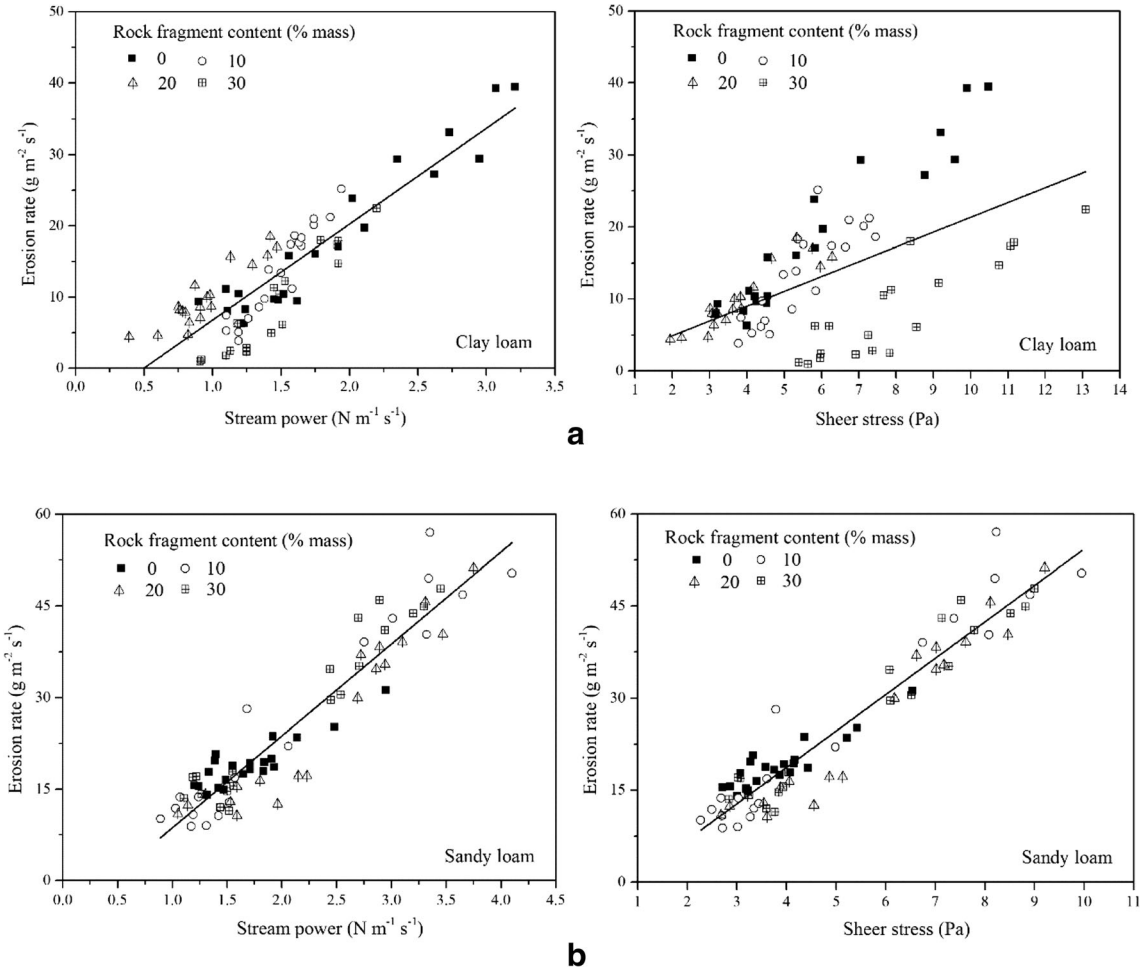

Fig. 11 Relationship between erosion rate and stream power/sheer stress for clay loam (**a**) and sandy loam (**b**) spoil heaps ($n = 79$)

13.349 for clay loam and 15.036 for sandy loam, suggesting a higher rate of increase of sandy loam erosion rate than clay loam erosion as stream power built up. The critical stream power levels of clay loam were 0.494 s^2 m^{-2} and 0.426 N m^{-1} s^{-1} for sandy loam spoil heaps (Table 3), indicating a greater soil resistance of the clay loam spoil heaps to scouring flow erosion. Meanwhile, the critical sheer stress of sandy loam was 0.840 Pa according to the equation. Figure 12 illustrates that the validation data points fit the 1:1 line well, demonstrating the high quality of the equations obtained in this study.

4 Discussion

4.1 Erosion process of spoil heaps

Due to the particular properties of spoil heaps, including composition materials and structure, erosion rate fluctuated differently over time in the experiments. This behavior is very different from that of the original landform, in which detachment is rapidly stabilized (Wen et al. 2015; Zhang et al. 2017). Loose soil coupled with scouring conditions made the rill erosion very intense on spoil heap slopes, and the recurrence of forming-shaping-stabilizing process of rills was the main

Table 3 Regression results of hydraulic parameters and erosion rates and the statistic evaluations

Soil	Hydraulic parameter	Equation	F ratio	p value	R^2	NSE	NRMSE
Clay loam	ω	$E_r = 13.349(\omega - 0.494)$	260.424	0.000	0.769	0.826	0.322
	τ	$E_r = 2.054(\tau + 0.387)$	36.866	0.000	0.315	0.491	0.550
Sandy loam	ω	$E_r = 15.036(\omega - 0.426)$	627.797	0.000	0.889	0.899	0.149
	τ	$E_r = 5.925(\tau - 0.840)$	818.558	0.000	0.913	0.928	0.125

reason for erosion rate fluctuation (Di Stefano et al. 2017). Previous studies have suggested that the side wall formed by rill erosion readily collapses under its own weight when subjected to scour action (Elliot and Laflen 1993; Han et al. 2011) which is another important reason for the great fluctuations in erosion rates.

The addition of rock fragments made the erosion rate change less fluctuating for clay loam but more sharply for sandy loam heaps (Fig. 6). The presence of rock fragment reduced soil cohesion in soil cross section, making it easier for the rill side collapse when lateral erosion was proceeding after undercutting, but it prevented the undercutting of rills. Thus, for clay loam, the extremely deep rills that always developed when the gravel content is 0% were not observed anymore; but for sandy loam, side wall collapsed more frequently when rock fragments increased despite the reducing undercutting. Previous findings have indicated that side wall slumping is related to the principles of soil mechanics and physics and tends to occur in soils with low cohesion and compressibility and high capillary pressure (Grabowski et al. 2011; Mahalder et al. 2018). This is consistent with our results, where the clay loam with higher cohesion and more aggregate retarded flow and resulted in less rill erosion and sediment yield with increasing rock fragments than the sandy loam (Fig. 10). As to the more severe rill development with adding rock fragments for sandy loam heaps, soil moisture content is an important factor in addition to the soil cohesion reduction. Previous research has demonstrated the importance of soil moisture content in erosion, with the plasticity index (PI) being a comprehensive indicator (Hanson and Hunt 2007). Higher PI values indicate soils in a plastic state over a wider range of water content (Rahimnejad and Ooi 2017); thus, soils that form more stable side walls have greater erosion resistance. In this study, clay loam had a higher PI than sandy loam due to its greater content of fine soil particles (< 0.002 mm). When the moisture content of the sandy loam exceeded its lower liquid limit (LLL), it was reduced to a viscous, sludge-like material (Fig. 7) prone to both collapsing and scouring, and the more rock fragments are contained, the more likely the structure to collapse. This explains the intense increase in erosion rate (Fig. 6) and rill width (Fig. 9) of the sandy loam spoil heaps in the later scouring period.

In the present study, the effect of rock fragment content on erosion depended on soil type: acceleration in sandy loam and conservation in clay loam (Fig. 8). This is different from the findings of Chow and Rees (1995) and Rieke-Zapp et al. (2007)

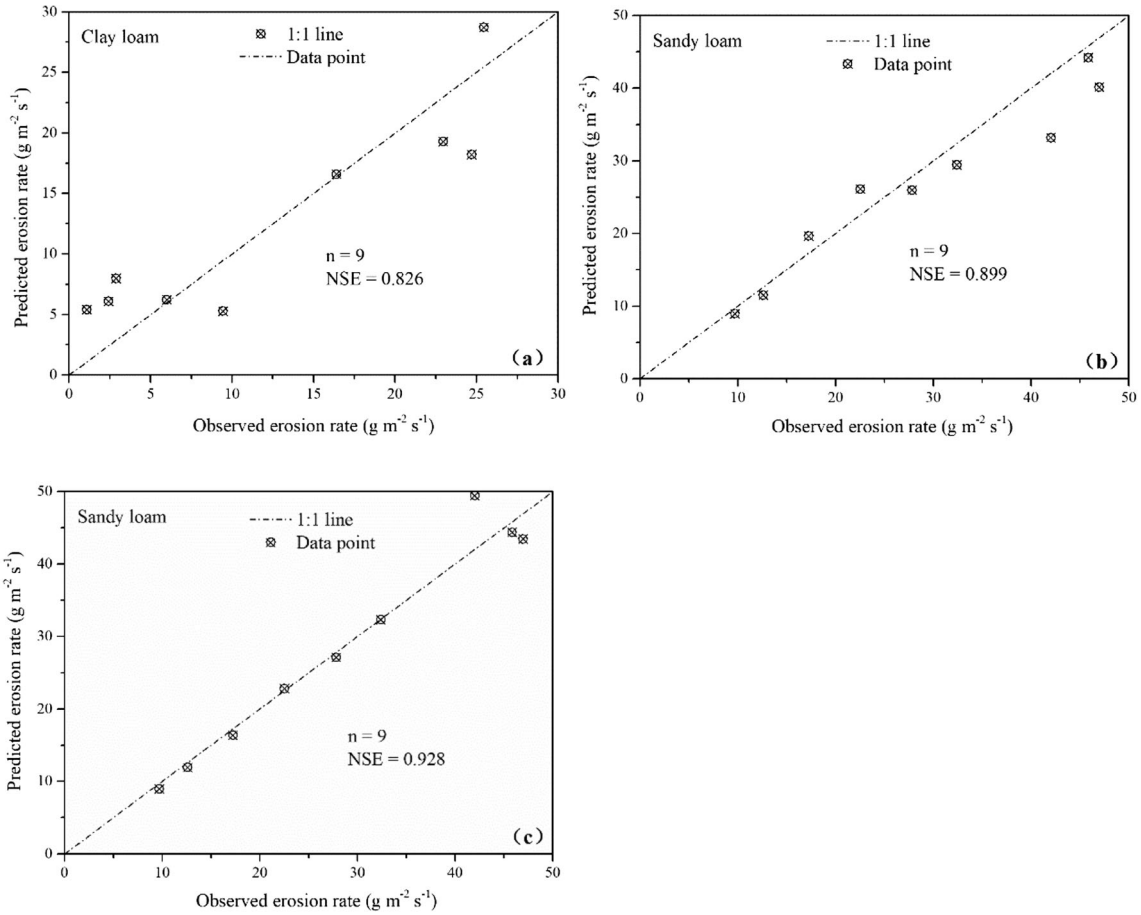

Fig. 12 Comparison of the observed and simulated values of erosion rates for different variations of stream power (**a**, **b**) and sheer stress (**c**)

that the increasing rock fragment proportion reduced sediment yield in agricultural fields, or what Li et al. (2017) concluded that soil loss was maximal in 25% gravel content and gradually declined for gravel content beyond 25% in mountain yellow-brown soil. Soil structure in spoil heaps was destroyed by severe disturbance, and the erosion mechanisms and effects of rock fragment content on infiltration and runoff yield are inconsistent with those of the undisturbed slope. Weak structural stability made spoil heaps easily to be eroded and tend to develop gullies when subjected to scouring; but based on the different physical properties of soils, the multiple effects of rock fragments performed differently.

Rock fragment content also can influence soil erosion by affecting the runoff which causes erosion and also transports the eroded sediment (Gordillo Rivero et al. 2015). Previous studies have shown that increased rock fragment content embedded in soil produces increased runoff in loamy sand mixing with a silica silt (Poesen et al. 1990). Zhou et al. (2009) found that solution infiltration rates decreased when rock fragment content was less than 40% and increased when more than 40% in loess soil. The present study shows that the added rock fragments linearly promoted runoff in sandy loam but impeded runoff in clay loam spoil heaps (Fig. 5), which was consistent with the sediment yield variation. The change in runoff yield with rock fragment content depended on the corresponding infiltration capacity. Increased rock fragment content increased the number of macropores and interstices between rock fragments and the surrounding fine earth, which is conducive to water infiltration but which may reduce the available infiltration cross-sectional area and increase flow path tortuosity, both of which tend to retard water infiltration. When the former effect is greater than the latter, runoff volume decreases, and vice versa (Cerdà 2001; Zhou et al. 2011; Hlaváčiková et al. 2015). For clay loam, due to its finer particles (clay particle content was 57.62%), soil pores were fine and distributed evenly with low permeability. When rock fragments were added into it, long and well-connected preferential flow channels had been developed because of the interfaces between soil and rock which increased the infiltration efficiently; at the same time, the negative impacts of rock fragments were not significant in clay loam because of the original slow vertical infiltration rate of the fine earth. However, for sandy loam, its large content of sand particle (83.91%) made a lot pores favorable for infiltration and better permeability. Although the rock fragments in it further increased the number of macropores, the promotion effect on infiltration of rock fragment was not obvious, because when there were a large number of macropores in the soil, the water tended to be stored in the macropores which increased the water holding capacity of the soil; only until the soil layer was saturated, the wetting front would continue to transport (Zhu and Shao. 2010). Meanwhile, for sandy loam with good infiltration itself, rock fragments cross cut the infiltration section and guided the lateral flow in soil to reduce vertical infiltration, and increased the runoff. But still, runoff production on spoil heap slopes with different rock fragment content conditions for different soil types needs further investigation.

Present results also showed that the effect of rock fragment cover became important in the later scouring stage by decreasing the erosion rate (Fig. 6) in both soil types, which confirmed the previous results (Abrahams et al. 2015; Sadeghi et al. 2015). Thus, it is evident that the rock fragment content can produce multiple effects under different underlying conditions.

4.2 Hydraulic description of the erosion process

Rock fragments in spoil heap soils increase the complexity of the hydrological processes in the soil. Depending on the characteristics of the rock fragments, water redistribution and some soil hydrological processes are affected (Katra et al. 2008). In this study, the GRA and the regression equations both showed that stream power could simulate the erosion process that takes place in spoil heaps efficiently, and the sheer stress also was a proper parameter for sandy loam heaps.

Shear stress and stream power are most often adopted in hydraulic models for predicting soil detachment based on simple hydraulic indicators (Knapen et al. 2007). Shear stress expresses the driving force, whereas stream power represents the energy available for soil detachment. Elliot and Laflen (1993) combined head cut, side wall slumping, and rill scouring erosion as a single stream power term in a linear model that demonstrated that stream power is the best predictor of erosion rates, including all of the various forms of erosion that occur during the overall process. The stream power equations presented herein (Table 3) supported this which simulated terms for all of the erosion processes (scouring, head cut, side wall slumping, and slaking) triggered by the weak structural stability of spoil heaps for both soil types, but the sheer stress equation was only applicable for sandy loam spoil heaps.

The threshold concept states that "incision only occurs where a threshold of soil resistance is exceeded" (Horton et al. 1934). The critical stream power was 0.494 N m^{-1} s^{-1} in clay loam spoil heaps and 0.426 N m^{-1} s^{-1} in sandy loam spoil heaps. These values are three to ten times lower than those for undisturbed soil (Wu et al. 2010). This mathematical result again shows the proneness and severity of soil erosion of spoil heaps.

Although stream power has also been proposed as the most appropriate indicator of detachment in other studies about spoil heaps (Wang et al. 2015; Zhang et al. 2015), there are some differences between the forms of the stream power equations. Linear equations were obtained in the present study and in Zhang et al. (2015); however, Wang et al. (2015) obtained a power function equation between stream power and soil detachment rate. In the latter, the spoil heaps were subjected to

sheet erosion from beginning to end due to laminar flow, but in our study, rill erosion appeared to be the major source of detached sediment. Therefore, the erosion pattern was considered to be the main contributor to the differences.

Our results offer a remarkable understanding of soil erosion mechanisms in two spoil heaps that each consisted of a different soil type. The study also proposes appropriate hydraulic parameters describing the erosional process. This will help to establish prediction models of the disturbed surface. However, the present study was limited to testing the effect on erosion when a range of rock fragment mass content was mixed with each of the soils. Further research is therefore necessary for different rock fragment sizes, spatial heterogeneity, and gravitational erosion form in spoil heaps.

5 Conclusions

Four proportions of rock fragment content (0%, 10%, 20%, and 30% by mass) were added to clay loam and sandy loam spoil heaps in order to investigate the erosional characteristics that was caused. Rock fragment content affected soil erosion distinctly differently in the two soils. The average erosion rates for clay loam and sandy loam spoil heaps were 8.24–18.55 g m^{-2} s^{-1} and 19.33–29.55 g m^{-2} s^{-1}, respectively, which rose linearly for sandy loam but fell linearly for clay loam spoil heaps with increasing rock fragment content. The physical properties of soil and loose structure of spoil heaps plus effects of rock fragments made the erosion rate evolution curves fluctuate greatly under scouring condition, reflecting the particularity of the erosion process of spoil heaps.

During each test, the average rates of increasing rill width were 4–5 mm min^{-1} and 6–9 mm min^{-1} for clay loam and sandy loam spoil heaps, respectively. Rill development in clay loam spoil heaps mainly occurred in the early period of erosion, while for sandy loam, the rills widened intensely in the later scouring stage. Concomitant with the change of erosion rate, rill development was weakened with increasing rock fragment content in clay loam but was improved in sandy loam.

Stream power described the soil erosion rate well for both soil types, and sheer stress also did well for sandy loam in this study. All the relationships were linear for both soils. The critical stream power in clay loam was 0.068 N m^{-1} s^{-1} greater than that in sandy loam. These findings imply that spoil heaps of sandy loam are prone to more severe erosion than spoil heaps of clay loam.

Acknowledgements This work was supported by the Natural Science Foundation of China (41601300), the West Light Foundation of the Chinese Academy of Sciences (XAB2015B06), and the Fundamental Research Funds for the Central Universities (2452016107).

References

Abrahams AD, Gao P, Aebly FA (2015) Relation of sediment transport capacity to stone cover and size in rain-impacted interrill flow. Earth Surf Process Landf 25:497–504

Basile PA, Riccardi GA, Zimmermann ED, Stenta AHR (2010) Simulation of erosion-deposition processes at basin scale by a physically-based mathematical model. Int J Sediment Res 25:91–109

Cerdà A (2001) Effects of rock fragment cover on soil infiltration, interrill runoff and erosion. Eur J Soil Sci 52:59–68

Chow TL, Rees HW (1995) Effects of coarse-fragment content and size on soil erosion under simulated rainfall. Can J Soil Sci 75:227–232. https://doi.org/10.4141/cjss95-031

Deng JL (1989) Introduction to Grey system theory. J Grey Syst 1:1–24

Di Stefano C, Ferro V, Palmeri V, Pampalone V (2017) Measuring rill erosion using structure from motion: A plot experiment. CATENA 156:383–392. https://doi.org/10.1016/j.catena.2017.04.023

Elliot WJ, Laflen JM (1993) A process-based rill erosion model. Trans ASAE 36:65–72

Fang H, Sun L, Tang Z (2015) Effects of rainfall and slope on runoff, soil erosion and rill development: an experimental study using two loess soils. Hydrocarb Process 29:2649–2658

Gilley JE, Gee GW, Bauer A, Willis WO, Young RA (1977) Runoff and erosion characteristics of surface-mined sites in Western North Dakota. Trans ASAE 20(697–700):704

Gordillo Rivero ÁJ, García Moreno J, Jordán A, Zavala LM, Granja Martins FM (2015) Fire severity and surface rock fragments cause patchy distribution of soil water repellency and infiltration rates after burning. Hydrol Process 28:5832–5843

Grabowski RC, Droppo IG, Wharton G (2011) Erodibility of cohesive sediment: the importance of sediment properties. Earth Sci Rev 105:101–120

Guo TL, Wang QJ, Li DQ, Jie Z (2010) Effect of surface stone cover on sediment and solute transport on the slope of fallow land in the semi-arid loess region of northwestern China. J Soil Sediment 10:1200–1208. https://doi.org/10.1007/s11368-010-0257-8

Han P, Ni J-R, Hou K-B, Miao C-Y, Li T-H (2011) Numerical modeling of gravitational erosion in rill systems. Int J Sediment Res 26:403–415

Hancock GR, Crawter D, Fityus SG, Chandler J, Wells T (2008) The measurement and modelling of rill erosion at angle of repose slopes in mine spoil. Earth Surf Process Landf 33:1006–1020

Hanson GJ, Hunt SL (2007) Lessons learned using laboratory JET method to measure soil erodibility of compacted soils. Appl Eng Agric 23:305–312

Harbor J (1999) Engineering geomorphology at the cutting edge of land disturbance: erosion and sediment control on construction sites. Geomorphology 31:247–263

Hlaváčiková H, Novák V, Holko L (2015) On the role of rock fragments and initial soil water content in the potential subsurface runoff formation. J Hydrol Hydromech 63:71–81

Horton RE, Leach HR, Vliet RV (1934) Laminar sheet-flow. Trans Am Geophys Union 15:393–404

Jomaa S, Barry DA, Brovelli A, Heng BCP, Sander GC, Parlange JY, Rose CW (2012) Rain splash soil erosion estimation in the presence of rock fragments. Catena 92:38–48

Kang HL, Wang WL, Li JM, Bai Y, Xue ZD, Deng LQ, Guo MM, Li YF (2016) Experimental study on runoff and sediment yield from engineering deposition with gravel in the northern windy-sandy region, Shaanxi. (in Chinese). Adv Water Sci 27:256–265

Katra I, Lavee H, Sarah P (2008) The effect of rock fragment size and position on topsoil moisture on arid and semi-arid hillslopes. Catena 72:49–55

Kayet N, Pathak K, Chakrabarty A, Sahoo S (2018) Evaluation of soil loss estimation using the RUSLE model and SCS-CN method in hillslope mining areas. Int Soil Water Conserv Res 6:31–42

Knapen A, Poesen J, Govers G, Gyssels G, Nachtergaele J (2007) Resistance of soils to concentrated flow erosion: a review. Earth-Sci Rev 80:75–109

Li G, Abrahams AD, Atkinson JF (1996) Correction factor in the determination of mean velocity of overland flow. Earth Surf Process Landf 21:509–515

Li T, He B, Chen Z, Zhang Y, Liang C (2017) Effects of gravel on concentrated flow hydraulics and erosion in simulated landslide deposits. Catena 156:197–204

Ma DH, Shao MA (2008) Simulating infiltration into stony soils with a dual-porosity model. Eur J Soil Sci 59:950–959. https://doi.org/10.1111/j.1365-2389.2008.01055.x

Mahalder B, Schwartz J, Palomino AM, Zirkle J (2018) Relationships between physical-geochemical soil properties and erodibility of streambanks among different physiographic provinces of Tennessee, USA. Earth Surf Process Landf 43:401–416

Misra RK, Rose CW (1996) Application and sensitivity analysis of process-based erosion model GUEST. Eur J Soil Sci 47:593–604

Morgan RPC, Quinton JN, Smith RE, Govers G, Poesen J, Auerswald K, Chisci G, Torri D, Styczen ME (1998) The European Soil Erosion Model (EUROSEM): a dynamic approach for predicting sediment transport from fields and small catchments. Earth Surf Process Landf 23:527–544

Nasri B, Fouché O, Torri D (2015) Coupling published pedotransfer functions for the estimation of bulk density and saturated hydraulic conductivity in stony soils. Catena 131:99–108

Nearing MA, Foster GR, Lane LJ, Finkner SC (1989) A process-based soil erosion model for USDA water erosion prediction project technology. Am Soc Agric Eng 32:1587–1593

Nearing MA, Polyakov VO, Nichols MH, Hernandez M, Li L, Zhao Y, Armendariz G (2017) Slope-velocity equilibrium and evolution of surface roughness on a stony hillslope. Hydrol Earth Syst Sci 21: 3221–3229

Nyssen J, Mitiku H, Poesen J, Deckers J, Moeyersons J (2001) Removal of rock fragments and its effect on soil loss and crop yield, Tigray, Ethiopia. Soil Use Manage 17:179–187. https://doi.org/10.1111/j.1475-2743.2001.tb00025.x

Nyssen J, Poesen J, Moeyersons J, Luyten E, Veyret-Picot M, Deckers J, Haile M, Govers G (2002) Impact of road building on gully erosion risk: a case study from the northern Ethiopian highlands. Earth Surf Process Landf 27:1267–1283

Peng X, Shi D, Jiang D, Wang S, Li Y (2014) Runoff erosion process on different underlying surfaces from disturbed soils in the Three Gorges Reservoir area, China. Catena 123:215–224

Poesen J, Ingelmo-Sanchez F, Mucher H (1990) The hydrological response of soil surfaces to rainfall as affected by cover and position of rock fragments in the top layer. Earth Surf Process Landf 15:653–671

Rahimnejad R, Ooi PSK (2017) Model for the erosion rate curve of cohesive soils. Transp Res Rec 2657:19–28

Rieke-Zapp D, Poesen J, Nearing MA (2007) Effects of rock fragments incorporated in the soil matrix on concentrated flow hydraulics and erosion. Earth Surf Process Landf 32:1063–1076

Sadeghi SHR, Gholami L, Sharifi Moghadam E, Khaledi Darvishan A (2015) Scale effect on runoff and soil loss control using rice straw mulch under laboratory conditions. Solid Earth 6:1–8

Shi ZJ, Xu LH, Wang YH et al (2012) Effect of rock fragments on macropores and water effluent in a forest soil in the stony mountains of the Loess Plateau, China. Afr J Biotechnol 11: 9530–9361. https://doi.org/10.5897/AJB12.145

Tommervik H, Johansen B, Hogda KA, Strann KB (2012) High-resolution satellite imagery for detection of tracks and vegetation damage caused by all-terrain vehicles (ATVs) in Northern Norway. Land Degrad Dev 23:43–52

Trenouth WR, Gharabaghi B (2015) Event-based soil loss models for construction sites. J Hydrol 524:780–788

Urbanek E, Shakesby RA (2009) Impact of stone content on water movement in water-repellent sand. Eur J Soil Sci 60:412–419. https://doi.org/10.1111/j.1365-2389.2009.01128.x

Wang XS, Xie YS, Chen X, Tian F (2015) Effects of rock fragment on soil erosion rule of engineering pyramidal accumulation in northern Jiangxi. (in Chinese). J Sediment Res 1:67–74

Wang XS, Chen X, Ma HC, Xie YS (2016) Hydrodynamic characteristics of engineering spoil bank slopes in the red soil region of northern Jiangxi Province, China. (in Chinese). Adv Water Sci 27:412–422

Wen L, Zheng F, Shen H, Bian F, Jiang Y (2015) Rainfall intensity and inflow rate effects on hillslope soil erosion in the Mollisol region of Northeast China. Nat Hazards 79:381–395

Wischmeier WH, Smith DD (1978) Predicting rainfall erosion losses—a guide to conservation planning. USDA, Agric Handbook 537. http://eprints.icrisat.ac.in/8473/1/RP_00210_Predicting_rainfall_erosion.....pdf

Wu SF, Wu P, Song WX, Bu CF (2010) Hydrodynamic process of soil detachment by surface runoff on loess slope. (in Chinese). Acta Pedol Sin 47:223–228. https://doi.org/10.11766/trxb200907210326

Zhang LT, Gao ZL, Yang SW, Li YH, Tian HW (2015) Dynamic processes of soil erosion by runoff on engineered landforms derived from expressway construction: a case study of typical steep spoil heap. Catena 128:108–121

Zhang Z, Li Q, Liu G, Tuo D (2017) Soil resistance to concentrated flow and sediment yields following cropland abandonment on the Loess Plateau, China. J Soils Sediments 17:1662–1671

Zhao X, Xie YS, Jing MX, Yang YL, Li WH (2012) Standardization parameter for spoilbank underlying surface simulation of development construction project (in Chinese). J Soil Water Conserv 26: 229–234. https://doi.org/10.13870/j.cnki.stbcxb.2012.05.029

Zhou BB, Shao MA, Shao HB (2009) Effects of rock fragments on water movement and solute transport in a Loess Plateau soil. Compt Rendus Geosci 341:462–472

Zhou BB, Shao MA, Wang QJ, Yang T (2011) Effects of different rock fragment contents and sizes on solute transport in soil columns. Vadose Zone J 10:386

Zhu YJ, Shao MA (2010) Simulation of rainfall infiltration in stony soil. Adv Water Sci 21:779–787 (in Chinese)